Analyst

RSC Publishing

PAPER

View Article Online
View Journal | View Issue

Cite this: *Analyst*, 2013, **138**, 4585

Label-free, high-throughput, electrical detection of cells in droplets†

Evelien W. M. Kemna,* Loes I. Segerink, Floor Wolbers, István Vermes and Albert van den Berg

Today, droplet based microfluidics has become a standard platform for high-throughput single cell experimentation and analysis. However, until now no label-free, integrated single cell detection and discrimination method in droplets is available. We present here a microfluidic chip for fast (>100 Hz) and label-free electrical impedance based detection of cells in droplets. The microfluidic glass-PDMS device consists of two main components, the droplet generator and the impedance sensor. The planar electrode pair in the main channel allows the detection of only cells and cell containing droplets passing the electrodes using electrical impedance measurements. At a measurement frequency of 100 kHz non-viable cells, in low-conducting (LC) buffer, show an increase in impedance, due to the resistive effect of the membrane. The opposite effect, an impedance decrease, was observed when a viable cell passed the electrode pair, caused by the presence of the conducting cytoplasm. Moreover, we found that the presence of a viable cell in a droplet also decreased the measured electrical impedance. This impedance change was not visible when a droplet containing a non-viable cell or an empty droplet passed the electrode pair. A non-viable cell in a droplet and an empty droplet were equally classified. Hence, droplets containing (viable) cells can be discriminated from empty droplets. In conclusion, these results provide us with a valuable method to label-free detect and select viable cells in droplets. Furthermore, the proposed method provides the first step towards additional information regarding the encapsulated cells (*e.g.*, size, number, morphology). Moreover, this all-electric approach allows for all-integrated Lab on a Chip (LOC) devices for cell applications using droplet-based platforms.

Received 22nd March 2013
Accepted 16th May 2013

DOI: 10.1039/c3an00569k

www.rsc.org/analyst

1 Introduction

Analysing single cells and performing biological studies on a single cell basis are of increasing interest.[1,2] Droplet-based microfluidics has become a standard platform for high-throughput single cell experimentation and analysis,[3–5] such as cell based assays,[6] polymerase chain reactions,[7] proteome analysis[8] and cell printing technologies.[9] Droplets facilitate high-throughput single cell analysis within micrometer-sized droplets,[10] which are physically and (bio)chemically isolated.[11] In addition, the uptake of trace chemicals can be probed because of the limited droplet volume and associated depletion of these chemicals. Using microfluidic devices, monodisperse droplets can be generated, merged, and sorted at kHz rates, enabling high-throughput single cell screening.[2] However, until now, label-free characterization and identification of cells in droplets, which is of great importance for cell analysis in droplets and selection of the droplets of interest, have not been demonstrated.

Single cell encapsulation has been developed into an integral part in droplet microfluidics. Therefore, deterministic encapsulation of single cells in droplets receives growing interest. We have demonstrated high-yield (77%) and high-speed (2700 cells per s) single cells in droplet encapsulation using Dean-coupled inertial ordering in a simple curved continuous microchannel.[12] However, 100% efficiency was not obtained, and it is difficult to reach due to the significant standard deviation in the longitudinal spacing between the cells. This inefficiency has stimulated us to develop a label-free method, using impedance, for the downstream selection of single cell containing droplets, to finally obtain 100% efficiency. As no cell labeling is required, the use of external optical equipment is avoided.[13,14] Although fluorescent labeling permits molecular-level detection, this technique is expensive, laborious and time consuming. Moreover, fluorescence detection is not easily integrated on chip.[15] Label-free on-demand impedance based cell encapsulation has been demonstrated by Lin *et al.*, but with relatively low throughput (10 Hz) and with the need for using valves.[16] Additionally, a droplet platform for cell detection in droplets has never been used.[17,18]

BIOS, Lab on a Chip group, MESA+ Institute for Nanotechnology, University of Twente, P.O. Box 217, 7500 AE Enschede, The Netherlands. E-mail: e.w.m.kemna@utwente.nl; Tel: +31 53 489 4782

† Electronic supplementary information (ESI) available. See DOI: 10.1039/c3an00569k

We present here a fast, novel and label-free impedance based approach to detect cells in droplets. A microfluidic glass-PDMS device is developed, consisting of two main components, the droplet generator and the impedance sensor. The droplet generator has a flow focusing structure for stable droplet generation and cell encapsulation. The impedance sensor comprises two planar electrodes, patterned on glass, positioned in the main channel. In this article, we demonstrate the differentiation between empty and cell encapsulated droplets, with the use of electrical impedance measurements at a single frequency.

Firstly, the chip design and the measurement set-up are described with a theoretical explanation. Secondly, the impedance spectra of single cells (viable *vs.* non-viable), empty droplets and cell-containing droplets are shown in either conducting (PBS) or iso-osmolar low-conducting (LC) buffer. We demonstrate that LC droplets encapsulating viable cells can be discriminated from empty droplets or droplets with non-viable cells, using high-speed impedance measurement analysis. To validate the impedance measurements, simultaneous high-speed camera recordings were taken for each measurement to ensure that cells were actually encapsulated and compared with the electrical signal.

2 Materials and methods

2.1 Chip design

The microfluidic chip consists of two main components, the droplet generator, with one inlet for the cell suspension and one inlet for the oil, and the impedance sensor. The droplet generator has a flow focusing junction with a width of 30 or 40 μm and a focus-width of 25 μm. Hence, the main channel is 30 or 40 μm wide. The impedance sensor comprises two planar platinum (Pt) electrodes with a width of 20 μm and an inter-electrode distance of 30 μm patterned on glass. The total chip depth is 26 μm.

A silicon master design was drawn using Clewin (version 4.0.1) and fabricated using standard UV-lithography. SU-8 2-25 (Microchem, Berlin, Germany) was spun on the silicon master with a thickness of 26 μm. The chip was made in PDMS (Sylgard 184, Dow Corning, Midland, MI, USA). Curing and base agents were mixed at a ratio of 1 : 10 and degassed. PDMS was poured onto a silicon wafer, degassed, and cured at 60 °C for 24 hours. After curing, the inlet and outlet were punched using a dispensing tip (Nordson EFD, Maastricht, the Netherlands, ID 1.36 mm and OD 1.65 mm). Subsequently, the PDMS chip was sealed to a Pyrex glass slide with the patterned Pt electrodes using oxygen plasma (Harrick PDC-001, NY, USA). After sealing, the chip was placed at 60 °C for a minimum of 30 minutes.

2.2 Materials

Iso-osmolar LC buffer, based on a study of Steenbakkers *et al.*,[19] consisted of deionized water, supplemented with 280 mM inositol (Sigma, St. Louis, USA), 0.1 mM calcium acetate (Sigma), 0.5 mM magnesium acetate (Sigma) and 1 mM L-histidine (Sigma). The conductivity was adjusted, using deionized water, to 0.009 S m^{-1}. For the continuous phase, hexadecane (Sigma) with 1% Span80 (Sigma) was used. Polystyrene beads (Thermo scientific, Breda, The Netherlands) with a diameter of 11 μm were used in control experiments.

2.3 Cell culture

The mouse myeloma cell line NS-1 was a kind donation from ModiQuest, The Netherlands. Cells were grown in DMEM/F12 medium (Invitrogen, Grand Island, NY, USA), supplemented with 10% (v/v) fetal bovine serum (FBS; Invitrogen), 100 U mL^{-1} penicillin (Invitrogen), and 2 mM L-glutamine (Invitrogen) (= $DMEM^+$ medium). Cell cultures were sustained in a 5% CO_2 humidified atmosphere at 37 °C. NS-1 cells were split every 3–4 days at a ratio of 1 : 10. In the experiments, cells were suspended in PBS or LC buffer at the desired concentration prior to use. To induce cell death, NS-1 cells were put at 56 °C in LC buffer for 30 minutes. After washing and resuspension in LC buffer, viability was checked in an aliquot of the sample using propidium iodide (PI) (Sigma) at a final concentration of 10 μg mL^{-1} and Calcein AM (Sigma) at a final concentration of 2.5 μM.

2.4 Experimental set-up

The cell suspension and the oil were separately introduced into the microfluidic chip using two glass Hamilton syringes (Sigma), and connected to the two inlets with PEEK tubing (Vici, Schenkon, Switzerland, ID 0.5 mm and OD 1.59 mm). PEEK tubing was also connected to the outlet of the device and routed into a collection tube. Flow was driven at a constant volume rate by a syringe pump (neMESYS dosing units, Cetoni GmbH, Germany). A magnetic stir bar was inserted into the syringe containing the cell suspension, to prevent suspension settling during injection.

When conducting measurements on empty droplets, flow rates of 0.15–0.5 μL min^{-1} for water and 1.8–8 μL min^{-1} for the continuous phase were used. The droplets were generated ranging from 20 to 475 Hz at a frame rate of 3000 fps.

Secondly, for experimentation regarding cell containing droplets, the flow rate of the continuous phase varied between 0.2 and 2 μL min^{-1}. The aqueous flow rate, containing the cells, varied between 0.05 and 1 μL min^{-1} and the frame rate was set to 125–500 fps, to be able to increase the recording time.

The microfluidic chip was mounted on an X–Y–Z translation stage of an inverted wide fluorescence microscope (Leica DM IRM, Leica Microsystems, Wetzlar, GmbH, Germany). Illumination was supplied by a fiber optic illuminator (Leica KL 1500 LCD). A computer-controlled high-speed camera (Photron SA-3, West Wycombe, United Kingdom), with accompanied Photron software (Photron Fastcam Viewer), was used for image recording of droplets passing the electrode pair. All videos and images captured were analyzed with the image-processing program ImageJ (National Institute of Health, MD, USA) and compared with the obtained electrical signals.

2.5 System overview

The electrodes on the glass slide of the chip were connected to a printed circuit board using wire bonding, enabling a stable electrical connection.

A frequency sweep of the chip was performed such that the influence of the different components of the equivalent circuit was identified at frequencies ranging from 1000 Hz to 40 MHz. Using an impedance/gain phase analyser (Hewlett Packard 4194A) a bode plot of the chip filled with PBS or LC buffer, with or without (non)viable cells at high concentrations, was generated. During the frequency sweep, flow was induced using different sized droplets on both inlets.

An AC signal of 100 kHz and 6–14 V_{pp} was generated by the Zurich system (HF2IS, Zurich instruments) and transferred to one electrode on the chip. At the other electrode, a home-made current amplifier was placed to measure the current in order to determine the impedance. This signal was fed back to the Zurich system and captured with a sample frequency of 899–3700 Hz at the laptop. For data analysis to calculate the impedance, Matlab (R2010B, version 7.11.0.854, 2010, Mathworks, Inc.) was used. The peak heights were detected and calculated, with respect to the baseline, such that the drift of the signal did not influence the analysis.

2.6 Matlab simulation

A model was used to determine the influence of the viability of the cell, suspended in LC buffer, on the frequency behavior of the impedance. Three different situations were modeled: (1) only an electrolyte present between the electrodes; (2) a viable cell between the electrodes and (3) a polystyrene bead between the electrodes. The cell was represented in the model as a single-shell model,[20–22] while the influence of the suspended bead was calculated using the Maxwell–Wagner theory.[20,21,23]

Using Matlab (R2010B, version 7.11.0.854, 2010, Mathworks, Inc.), a bode plot of the three different situations was made. The conductivity and permittivity of the LC buffer were set to 0.009 S m^{-1} and 80 × ε_0, respectively ($\varepsilon_0 = 8.854 \times 10^{-12}$ F m^{-1}). Based on the data of Sun and Morgan in 2010,[22] the parameters used for the cell were 7.5 μm for the cell radius, 1×10^{-8} S m^{-1} for the conductivity membrane, 0.4 S m^{-1} for the conductivity cytoplasm, and 5 × ε_0 and 60 × ε_0 for the relative permittivity of the cell membrane and cytoplasm, respectively ($\varepsilon_0 = 8.854 \times 10^{-12}$ F m^{-1}). For the polystyrene beads (radius, 5.5 μm) the values were 2.5 × ε_0 and 1×10^{-16} S m^{-1} for the relative permittivity and conductivity. The membrane thickness was set to 5 nm.

3 Results and discussion

3.1 The microfluidic device

3.1.1 Equivalent circuit model and system overview. Electrical impedance spectroscopy measures the AC electrical properties of particles (in suspension) from which the dielectric parameters of the particles can be obtained.[22] Impedance analysis is a widely used method for label-free analysis of cells.[17,18,24,25]

The chip was connected with the Zurich impedance system (HF2IS, Zurich instruments) using a home-made current amplifier, to measure the current in order to determine the impedance. The chip was glued on a printed circuit board (Fig. 1A). A simplified equivalent circuit model for three different situations is given in Fig. 1B. In all situations, there are two double layer capacitances (C_{dl}), caused by the electrode–fluid interface, a parasitic capacitance (C_{par}) and a lead resistance (R_{lead}). When a droplet passes the electrode pair the double layer present in the oil changes to a double layer present in the buffer. Also the R_{oil} is interchanged for R_{drop}, consisting of the used buffer and C_{drop} is added. When the droplet contains a cell, an additional circuit for the cell is implemented. This is represented by the addition of an equivalent circuit model for a cell (capacitance of the cell membrane (C_{mem}) and resistance of the cell interior (R_{cell})). The components of the cell are frequency dependent. Primarily due to the presence of the cell membrane, the cell presents a different impedance measurement when compared to the surrounding fluid. This change is detected by the sensing electrodes and is used to indicate the presence of a cell inside a droplet. The membrane of a cell, suspended in conducting buffer, forms a barrier to the current flow at frequencies below 1–3 MHz. Below these frequencies, the cell can be seen as an insulating sphere, which causes an impedance change depending on the size of the cell.[16] However, for a cell suspended in LC buffer, the frequency at which the current flows through the interior of the cell is lower. For example for a buffer with a conductivity of 0.0016 S m^{-1} the frequency is expected to be around 10 kHz.[22]

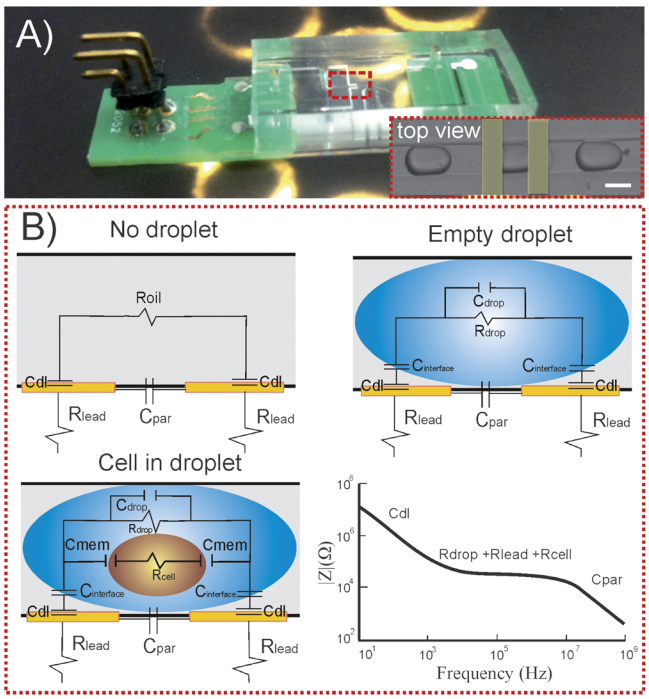

Fig. 1 (A) Photo of the microfluidic device glued on a printed circuit board. The inset shows the impedance sensor. Scale bar is 30 μm. (B) Simplified equivalent circuit model of the microfluidic device w/o droplet, or cell in droplet. The interface between the two planar electrodes and the buffer in oil droplet is represented by the double layer capacitance (C_{dl}). R_{drop} is the buffer resistance and C_{drop} is the buffer capacitance. R_{lead} is the lead resistance and C_{par} is the parasitic capacitance. The schematic bode plot shows a typical frequency response of the electrical impedance of the equivalent circuit model for the situation of a cell containing droplet.

A typical bode plot of the equivalent circuit model is shown in the bottom right corner of Fig. 1B. At low frequencies, the spectrum is influenced by the double layer capacitances. A resistive plateau is seen at intermediate frequencies, which is primarily caused by the resistances in the channel due to the buffer, droplet and/or cell. The parasitic capacitance plays a role at higher frequencies.

3.1.2 Characterization of the microfluidic device. The frequency behavior of the microfluidic chip with PBS or LC buffer, with and without (non)viable cells was determined to ensure that the electrical impedance measurements were performed at a frequency within the resistive plateau. Fig. 2A and B show the averaged results of 50 individual impedance measurements of a chip filled with PBS or LC buffer for frequencies from 1 kHz to 40 MHz. The bode plot for PBS shows a clear influence of the double layer capacitance and parasitic capacitance. The electrolyte resistance is represented in the shaded area, nevertheless the double layer and parasitic capacitance are almost interlaced. In the bode plot of the LC buffer, the influence of the double layer capacitance, electrolyte resistance and parasitic capacitance can be clearly distinguished. Again the shaded area represents the resistive area. The cutoff frequencies, F_1 and F_2, of the resistive area have been estimated using $F_1 \sim 1/(\pi \times R_{el} \times C_{dl})$ and $F_2 \sim 1/(2\pi \times R_{el} \times C_{par})$ by Langereis,[26] where, F_1 and F_2 of solely PBS are 129 kHz and 395 kHz, respectively. For LC buffer, F_1 and F_2 were 663 Hz and 2 MHz, respectively. These values were combined with the visual inspection of the obtained bode plots of the different buffers with or without viable and non-viable cells. The obtained bode plots are in correspondence with the previous described theory and show at lower frequencies the influence of the double layer capacitance, at higher frequencies the parasitic capacitance and in the middle the influence of the buffer between the electrodes in the channel. The addition of cells to the LC buffer changes the frequency behavior. The presence of non-viable cells in LC buffer between the electrodes increased the impedance. However, a decrease in impedance was observed when viable cells were suspended in LC buffer. These data suggest that when using LC buffer, the behavior of viable cells with respect to the LC buffer alone is opposite to the behavior of non-viable cells. Similar results were obtained when comparing these results with our model. Due to the presence of viable cells in LC buffer, the impedance decreases, compared to solely LC buffer between the electrodes, indicating that a viable cell acts as a conducting sphere in LC buffer around 100 kHz. Since the cell cytoplasm is more conducting, the cell can be seen as a conducting sphere in comparison to the surrounding LC buffer. Sun and Morgan[22] show pDEP for cells in LC buffer and at 100 kHz; this relates the cell cytoplasm conductivity to the surrounding medium. This results in the detection of a viable cell as a decrease in impedance. This different electrical behavior of the cells is due to the presence of LC buffer instead of conducting buffer, where cells behave as insulating spheres below 3 MHz.[22]

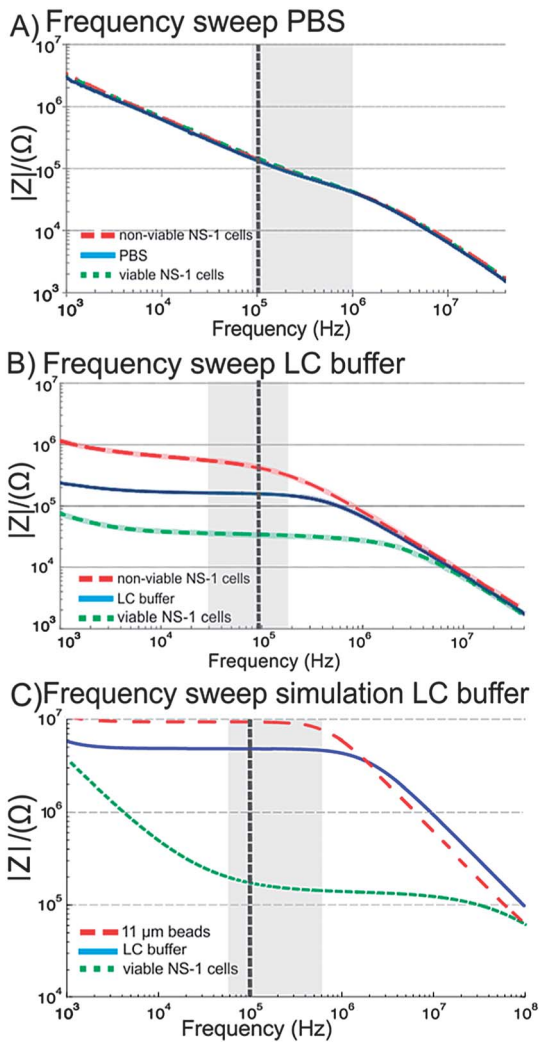

Fig. 2 The measured frequency behavior of the microfluidic chip. (A and B) The lines in the graph show the average of 50 measurements obtained with the impedance/gain phase analyser using either PBS or LC buffer with or without (non)viable NS-1 cells. The shaded area indicates the resistive plateau and the dashed line represents the measurement frequency used during all subsequent experiments. Variance between 50 measurements is shown by shaded lines. (C) Simulation of the frequency response of the electrical impedance of the equivalent circuit model with viable NS-1 cells, beads and only LC buffer.

Additionally, the influence of a solid sphere in the LC buffer was simulated, which resulted in a higher impedance at the resistive plateau. Beads were used in this simulation, since it was unclear what exactly happens with the equivalent electrical circuit model of a dead cell. Cell death was induced by heat and the compromised membrane allowed for cytoplasm leakage, leaving only a resistive membrane with denatured proteins. Therefore it was assumed that a non-viable cell can be represented as non-conducting membrane 'debris'. The modeled bead showed comparable results as non-viable cells, indicating that non-viable cells indeed act as resistive particles in LC buffer around 100 kHz.

When performing the frequency sweep measurements there was a highly concentrated cell containing solution present. This was transported through the device as described in Section 2.5. Therefore, the frequency sweep is based on a NS1 cell population. Moreover, the cells pass by at different positions in the

channel. Hence, this induces moderate variation in the measured impedance, therefore 50 measurements were performed, averaging the effect.

The difference between viable and non-viable cells was not shown around 100 kHz, using a conducting buffer (PBS), which makes the use of LC buffer favorable, offering the discrimination based on viability. Lowering the buffer conductivity, therefore changing the buffer properties and electrical behavior of cells lowers the frequencies at which discrimination between viability can be performed. Next, the frequency ranges in the shaded areas were examined and the optimal measurement frequency was shown to be at 100 kHz, for both PBS and LC buffers. So in further experiments, an actuation frequency of 100 kHz was used.

3.2 Droplet generation and detection

Droplets were generated using a flow focusing junction. Fig. 3A shows that the droplet generation frequency was determined with a maximum at 475 Hz and visually confirmed using high-speed recordings. The length and the frequency of the droplets were varied using a range of flow rates. In our measurement system, we were able to relate the electrical amplitude to the droplet length (Fig. 3B). Hence, the impedance change can be used to define an approximation of the droplet volume and detect changes in the droplet volume.

A quadratic power relationship between the droplet length and the measured impedance change is shown. This is due to the use of a first-order low-pass filter by the Zurich system. This filter suppresses the changes caused by the fast events, such as the passage of the droplet. For a long droplet, these changes occur at a lower frequency than for shorter droplets, and therefore the effect is less, resulting in a larger impedance peak. Another reason for the relationship between the droplet length and impedance change could be the RC-time of the setup or the wetting of the electrodes. Furthermore, Fig. 3B shows that the measurement change of empty droplets passing one electrode pair can be used to determine the droplet length up to 185 μm. If the droplet length continuously increases the signal will saturate. At this point it is similar to measuring in solely (low) conducting buffer. Nevertheless, a passing cell will still result in an impedance change and can be detected. However, at a certain point there is plug flow and for our experiments and applications measuring cells in droplets is of crucial interest.

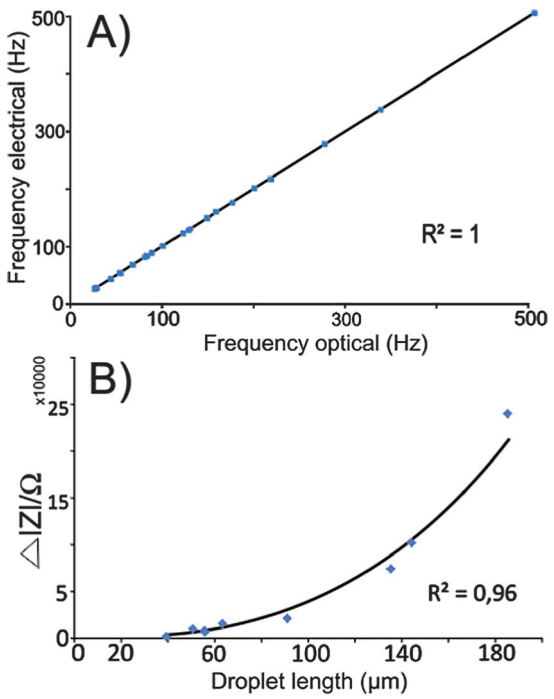

Fig. 3 (A) Optical *versus* impedance based droplet frequency determination. (B) Droplet length *versus* electrical amplitude obtained with the Zurich impedance system. Sample rate 899 Hz, F_{act} = 100 kHz, 16 V_{pp}.

3.3 Cell detection in different conducting buffers

NS-1 cells were suspended in LC buffer and measured at a frequency of 100 kHz and 6 V_{pp}. Both positive and negative peaks were observed, as shown in Fig. 4A.

When suspending solely non-viable cells, only positive peaks were observed, with an average impedance change of 24 400 ± 12 500 Ω (Fig. 4C). This indicates that non-viable cells in LC buffer give an increase in impedance, as described previously (Fig. 2). The opposite effect, an impedance decrease, was observed when a viable cell passed the electrode pair with an average of −60 400 ± 37 600 Ω (Fig. 4C). This peak height also corresponds to the cell volume, as shown in Fig. 4A, peak numbers 1 and 2 correspond to cells 1 and 2 in the inset. The decrease in resistance of viable cells in LC buffer can be explained by the presence of the conducting cytoplasm compared to the surrounding LC buffer. This results in an increase in the conductivity at the applied measurement frequency. As a consequence, the impedance decreases, giving rise to a negative peak. This effect is also confirmed by the simulations using Maxwell–Wagner theory (Fig. 2C). Cell death was induced by heat. After this the cells were washed and suspended in fresh LC buffer, thereby replacing the cytoplasm with LC buffer. The induced heat denatures proteins and changes the membrane properties. Hence, it is likely that the present membrane 'debris' adds to the impedance as a resistance at the measurement frequency, resulting in positive peaks. This observation is supported by the results shown in Fig. 4A and C, where non-viable cells show similar impedance changes, unrelated to the (original) cell volume, and the membrane 'debris' is measured.

This hypothesis is supported by the observation that 11 μm beads suspended in LC buffer behave similar to non-viable cells as shown in Fig. 4C. In conclusion, by using LC buffer it is possible to differentiate between viabilities based on the peak appearances. This is not possible when using more conducting buffer (PBS, 1.4 S m^{-1}). Data showed, for both viable and non-viable cells, positive peaks at frequencies ranging from 10 kHz to 3 MHz (Fig. 4B). Hence, NS-1 cells suspended in PBS at an actuation frequency of 100 kHz behave as insulating spheres, as expected.

To underline the possibility to detect a change in impedance when a cell containing droplet passes by, we have calculated

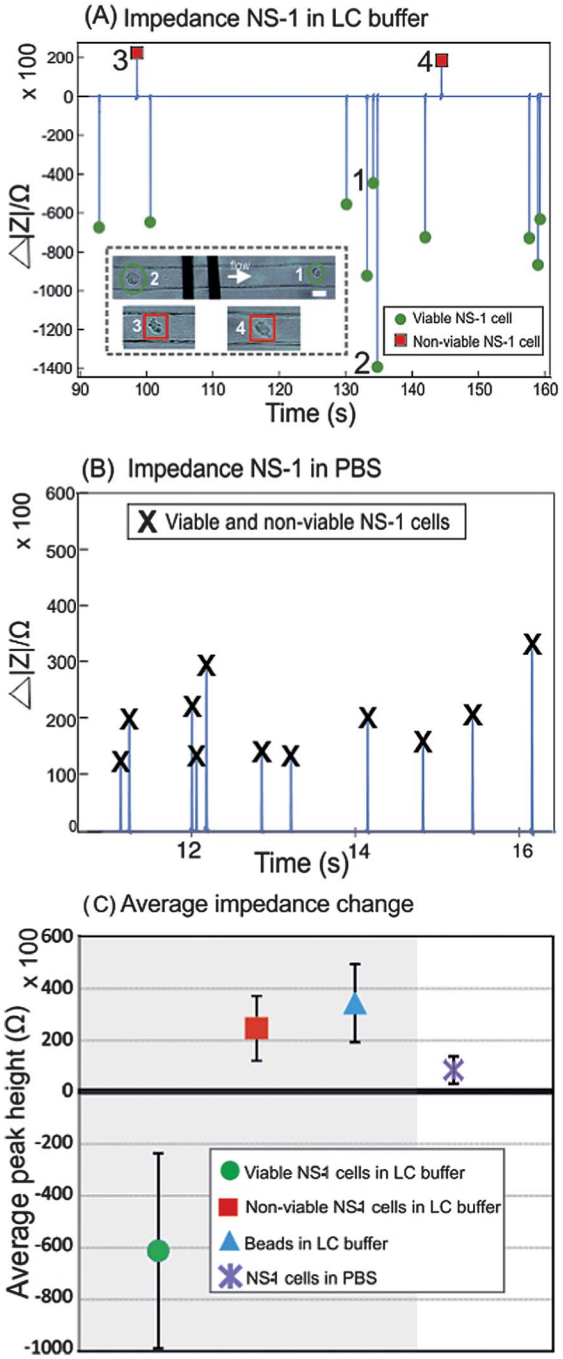

Fig. 4 (A) The processed signal with the peak heights and discrimination between viable and non-viable cells in buffer (Zurich impedance system sample rate 899 Hz, F_{act} = 100 kHz, 6 V_{pp}). The inset is a microscopic image of a viable small (1) and a viable large (2) NS-1 cell passing the electrode pair (black bars) and two non-viable cells (3) and (4). Scale bar is 20 μm. (B) The processed signal with the peak heights of NS-1 cells in PBS (Zurich impedance system sample rate 899 Hz, F_{act} = 100 kHz, 6 V_{pp}). (C) The average impedance change of viable cells (n = 68), non-viable cells (n = 154) and beads (n = 12) in either LC buffer (shaded area) or PBS (n = 38).

that the R_{cell} has a relative contribution of 9.6% to the total R (R_{cell} + R_{lead} + R_{drop}, see Fig. 1B). This is at a measurement frequency of 100 kHz in LC buffer, suggesting that it would be possible to detect an impedance change in a cell containing droplet compared to an empty droplet.

LC buffer is not a standard buffer to use in cell experiments, therefore the viability of NS-1 cells in LC buffer was evaluated. The viability of NS-1 cells, kept for 90 minutes in LC buffer, was ~95%. After two hours, the viability decreased significantly to 85% (data not shown).

3.4 Cell encapsulation and detection

Final experiments were focused on the detection of cells in droplets. Due to the best discriminating potency, NS-1 cells were suspended in LC buffer. Since LC buffer is more conducting than the continuous phase, the resistivity reduces when a droplet passes and thus the impedance signal decreases. As a result, empty droplets generate negative peaks.

Fig. 5 shows the detection of two cell containing droplets using the impedance measurement data. When a droplet contained a viable cell, a decrease in impedance was shown (see ESI Video 1†). Different signal data were generated, however it was observed that the real part of the obtained signal was the most stable and the change due to a cell containing droplet was the most significant. When the combined impedance signal was used, the signal contained more noise due to the added phase information, making it more difficult to differentiate between the base line (empty droplets) and peaks (cell containing droplets).

Cells in LC droplets were detected up to a droplet frequency of 112 Hz. Additionally, non-viable cells and beads encapsulated in LC droplets could not be detected based on impedance change. Moreover, it was not possible to differentiate between empty and cell containing PBS droplets, using frequencies ranging from 10 Hz to 5 MHz.

As mentioned in Section 3.2, the impedance change is related to the droplet length (therefore volume), so for discrimination based on the presence of a cell, it is of utmost importance to generate homogeneous droplets. This length or volume effect can also be observed in Fig. 5 right part (23.5 s), where the base line has a larger amplitude compared to the left part (6 s). At 6 s the volume of the droplets is 43 pL (n = 20) and at 23.5 s the volume of the droplets is 45.8 pL (n = 20).

To eliminate a possible effect of droplet volume on the impedance change of a cell encapsulating droplet, the length of empty droplets was measured (n = 20) and compared to the length of cell encapsulating droplets. The real part of the generated signal was used and the measurement of the empty and cell encapsulating droplet lengths using the corresponding frames showed no significant difference. However, the change in amplitude of signals generated by cell encapsulating droplets compared to empty droplets did significantly differ (p < 0.01). This finding eliminates the influence of the droplet length on the impedance change of the cell containing droplet, concluding that the measured change is solely based on the presence of a viable cell inside the droplet. Furthermore, data suggest that a droplet containing two cells causes a relatively larger impedance change, compared to a droplet which has only one cell. However, this difference is not significant, this is most likely due to the combined effects of *e.g.* cell number, cell size, position and viability.

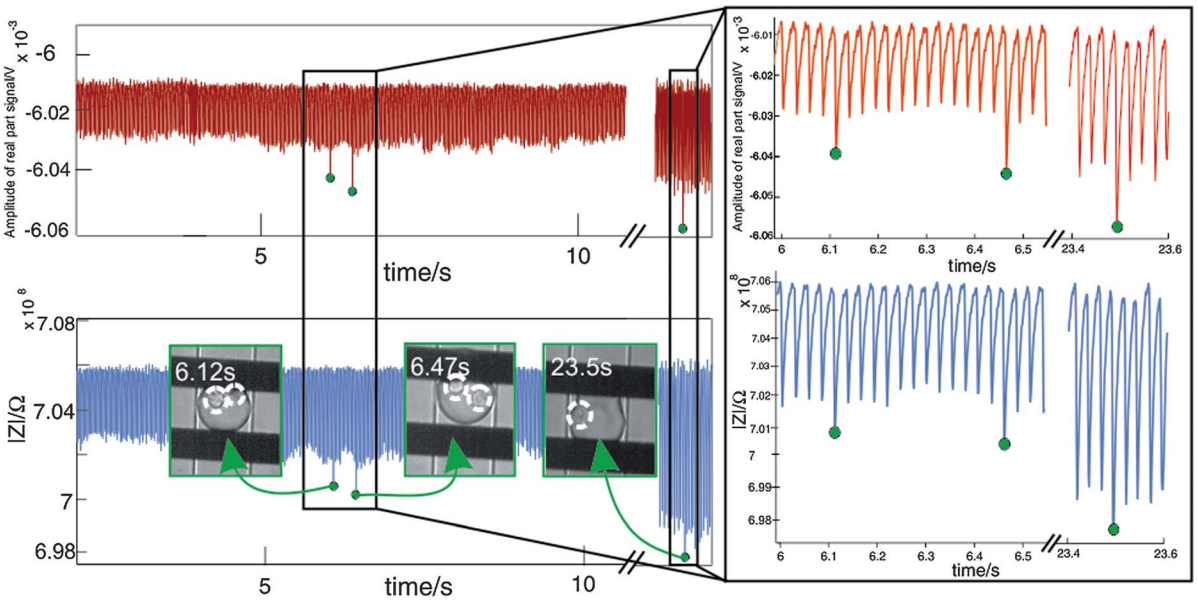

Fig. 5 NS-1 cell in droplet detection using real part of the voltage signal (top) and the final impedance change (bottom). NS-1 cells in LC buffer at F_{act} = 100 kHz, sample rate is 899 Hz and 6 V_{pp} obtained with the Zurich impedance system.

The sensitivity of the performed impedance measurements is 80%, hence 80% of the cell containing droplets are classified as a cell containing droplet using three times the standard deviation of empty droplets. Not all cell containing droplets were detected, which could be due to the cell position in the droplet or the sensitivity of the measurement setup. Finally, it could be due to the presence of non-viable cells instead of viable cells, because the viability of the cells in the LC buffer after encapsulation has been shown to be 90%. Furthermore, 99.98% of the empty droplet were correctly identified. Finally, a positive predictive value of 89% and a negative predictive value of 99.95% were shown (total amount of measured droplets is 8188).

Finally, the viability of the encapsulated cells was examined. The cells were stained with Calcein AM and propidium iodide to determine cell viability and membrane integrity after encapsulation. Results showed that 90% of the cells retained their membrane integrity after 90 minutes, compared with 95% in control samples (data not shown). When the electrical field of 100 kHz and 20 V_{pp} was switched on, the viability decreased to 91% (data not shown). So, there is no significant effect of the electric field on the viability of the cells when passing, for several milliseconds, an AC field of 100 kHz.[27] Furthermore, the LC buffer prevents localized heating.

4 Conclusions

Today, the analysis of single cells in droplets is of increasing interest. However, until now, it is not possible to characterize and identify cells in droplets, which is of utmost importance to select the droplets of interest. Here, a microfluidic device for the label-free detection of cells in droplets, based upon electrical measurements, is presented. To our knowledge, this is the first time that label-free detection of cells in droplets is shown. The device enables us to measure the individual volume, frequency and even content of the droplets.

Future experiments are focused on increasing the operating droplet frequency to several kilohertz, using a dedicated lock-in-amplifier. Furthermore, we want to detect cells in PBS or culture medium droplets, which is a better environment regarding the viability of cells, and favors cell culture in droplets. The sensitivity of the impedance measurement data can be increased by using parallel electrodes instead of planar ones and selection of the droplets of interest can be performed by incorporating a dielectrophoresis module.

Acknowledgements

Financial support from ERC (eLab4life project), Spinoza grant, Nanonext and technical assistance of J. G. Bomer, A. Sprenkels, M. Odijk and P. M. ter Braak are gratefully acknowledged. The authors declare no conflict of interest.

Notes and references

1 D. A. Weitz, *et al.*, Drop-based microfluidic devices for encapsulation of single cells, *Lab Chip*, 2008, **8**(7), 1110–1115.
2 E. Um, S. G. Lee and J. K. Park, Random breakup of microdroplets for single-cell encapsulation, *Appl. Phys. Lett.*, 2010, **97**(15), 153703-1–153703-3.
3 A. A. Bhagat, *et al.*, Inertial microfluidics for sheath-less high-throughput flow cytometry, *Biomed. Microdevices*, 2010, **12**(2), 187–195.
4 J. F. Edd, *et al.*, Controlled encapsulation of single-cells into monodisperse picolitre drops, *Lab Chip*, 2008, **8**(8), 1262–1264.

5 S. Koster, *et al.*, Drop-based microfluidic devices for encapsulation of single cells, *Lab Chip*, 2008, **8**(7), 1110–1115.
6 G. Gelinck, *et al.*, Charge transport in high-performance ink-jet printed single-droplet organic transistors based on a silylethynyl substituted pentacene/insulating polymer blend, *Org. Electron.*, 2011, **12**(8), 1319–1327.
7 S. H. Chao, *et al.*, Real-time PCR of single bacterial cells on an array of adhering droplets, *Lab Chip*, 2011, **11**(13), 2276–2281.
8 A. R. Wheeler, *et al.*, Digital microfluidics with in-line sample purification for proteomics analyses with MALDI-MS, *Anal. Chem.*, 2005, **77**(2), 534–540.
9 P. Koltay, *et al.*, Inkjet-like printing of single-cells, *Lab Chip*, 2011, **11**(14), 2447–2454.
10 J. Clausell-Tormos, *et al.*, Droplet-based microfluidic platforms for the encapsulation and screening of Mammalian cells and multicellular organisms, *Chem. Biol.*, 2008, **15**(5), 427–437.
11 E. Brouzes, *et al.*, Droplet microfluidic technology for single-cell high-throughput screening, *Proc. Natl. Acad. Sci. U. S. A.*, 2009, **106**(34), 14195–14200.
12 E. W. Kemna, *et al.*, High-yield cell ordering and deterministic cell-in-droplet encapsulation using Dean flow in a curved microchannel, *Lab Chip*, 2012, **12**(16), 2881–2887.
13 S. K. Y. Tang, *et al.*, A multi-color fast-switching microfluidic droplet dye laser, *Lab Chip*, 2009, **9**(19), 2767–2771.
14 L. I. Segerink, *et al.*, On-chip determination of spermatozoa concentration using electrical impedance measurements, *Lab Chip*, 2010, **10**(8), 1018–1024.
15 N. Bao, J. Wang and C. Lu, Recent advances in electric analysis of cells in microfluidic systems, *Anal. Bioanal. Chem.*, 2008, **391**(3), 933–942.
16 R. Lin, *et al.*, Novel on-demand droplet generation for selective fluid sample extraction, *Biomicrofluidics*, 2012, **6**(2), 024103-1–024103-10.
17 D. Holmes, *et al.*, Leukocyte analysis and differentiation using high speed microfluidic single cell impedance cytometry, *Lab Chip*, 2009, **9**(20), 2881–2889.
18 D. Holmes and H. Morgan, Single cell impedance cytometry for identification and counting of CD4 T-cells in human blood using impedance labels, *Anal. Chem.*, 2010, **82**(4), 1455–1461.
19 P. G. Steenbakkers, H. A. Hubers and A. W. Rijnders, Efficient generation of monoclonal antibodies from preselected antigen-specific B cells. Efficient immortalization of preselected B cells, *Mol. Biol. Rep.*, 1994, **19**(2), 125–134.
20 H. Morgan, *et al.*, High speed multi-frequency impedance analysis of single particles in a microfluidic cytometer using maximum length sequences, *Lab Chip*, 2007, **7**(8), 1034–1040.
21 K. R. Foster and H. P. Schwan, Dielectric-Properties of Tissues and Biological-Materials – a Critical-Review, *CRC Crit. Rev. Bioeng.*, 1989, **17**(1), 25–104.
22 T. Sun and H. Morgan, Single-cell microfluidic impedance cytometry: a review, *Microfluid. Nanofluid.*, 2010, **8**(4), 423–443.
23 J. C. Maxwell, *A treatise on electricity and magnetism*, Clarendon press, Oxford, 1873.
24 A. B. Cosimi, *et al.*, Immunologic monitoring with monoclonal antibodies to human T-cell subsets, *Transplant. Proc.*, 1981, **13**(3), 1589–1593.
25 W. P. Carney, *et al.*, Analysis of T lymphocyte subsets in cytomegalovirus mononucleosis, *J. Immunol.*, 1981, **126**(6), 2114–2116.
26 G. R. Langereis, *An integrated sensor system for monitoring washing processes*, University of Twente, 1999.
27 S. Archer, *et al.*, Cell reactions to dielectrophoretic manipulation, *Biochem. Biophys. Res. Commun.*, 1999, **257**(3), 687–698.

